Electron nuclear dynamics of $H^+ + H_2$ collisions at $E_{lab} = 30$ eV

Jorge Morales, Agustin Diz, E. Deumens, and Yngve Öhrn
Quantum Theory Project, University of Florida, Gainesville, Florida 32611

(Received 27 March 1995; accepted 6 September 1995)

Proton collisions with hydrogen molecules at 30 eV in the laboratory frame is a simple ion-molecule system exhibiting a number of distinct processes such as inelastic scattering, charge transfer, rearrangement, and dissociation. The electron nuclear dynamics (END) theory which allows full electron nuclear coupling and which does not restrict the system from reaching any of the possible product channels, is applied to this sytem to produce transition probabilities, differential, and integral (vibrationally resolved) cross sections. Comparisons with experiment demonstrate that END, even in its simplest implementation, with a single determinantal state for the electrons and with classical nuclei, yields results that are competitive with other theoretical approaches. © *1995 American Institute of Physics.*

I. INTRODUCTION

Surprisingly little is known at the present time about the dynamics of charge transfer in ion-molecule collisions. Conventional pictures of reactive collisions, such as charge transfer, involve transitions between two or more potential energy hypersurfaces and regions of configuration space where diabatic potential energy surfaces cross and where the Born–Oppenheimer approximation breaks down. The accurate determination of adiabatic or diabatic potential energy surfaces and their nonadiabatic coupling terms is a theoretically challenging and tedious undertaking and far from a routine task even for as simple cases as triatomic systems. The pointwise representation of adiabatic potential energy surfaces and their coupling terms must be fitted to some suitable analytical form, a far from trivial task, which can introduce errors that are hard to control. One can thus easily identify reasons for the scarcity of theoretical results for charge transfer dynamics. Similarly, there are experimental difficulties to overcome both in identification of product ions and neutral species as well as in their state selection.

The relatively recent study of vibrationally resolved charge transfer processes in proton hydrogen molecule collisions at 30 eV (laboratory frame) by Niedner, Noll, Toennies, and Schlier[1] with comparisons to theoretical investigations using the trajectory surface hopping model[2,3] (TSHM) has stimulated a quantum mechanical study of this system in three dimensions by Baer, Niedner-Schatteburg, and Toennies[4] using two diatomics-in-molecules (DIM) surfaces in internal coordinates and a transformation to diabatic surfaces and associated coupling terms. There is better agreement between experiment and theory using the quantum mechanical study than with the TSHM, but there are still some discrepancies in cross sections, both total and differential.

We present here a theoretical study of this simple collisional system using the electron nuclear dynamics (END) approach,[5,6] which does not employ potential energy surfaces but considers, in a limited electronic basis set, the full dynamics of electrons and nuclei under the influence of instantaneous mutual forces. In the following sections the results of this study are analyzed and presented. The agreement with experiment is excellent. This is encouraging since the calculations are carried out at the simplest level of the theory. In this sense, it follows the trend of other applications of END to ion-atom and other ion-molecule collisions.[7,8]

The END is an explicitly time-dependent theory and employs the time-dependent variational principle to develop a set of coupled first-order differential equations that approximate the time-dependent Schrödinger equation with the full many-particle Coulombic Hamiltonian for electrons and nuclei. A laboratory system of Cartesian coordinates is used avoiding the often cumbersome and limiting transformations to special internal coordinates. The dynamical equations fully account for electron-nuclear coupling terms and assume the form of Hamilton's equations on a generalized phase space.[9] The structure of these equations is discussed in the next section.

The reasons for the development of such a detailed dynamical theory as END and its implementation in the computer code ENDyne[10] are many. The more immediate motivation for that substantial undertaking is the growing evidence that the tools now exist to solve the time-dependent Schrödinger equation for systems of chemical interest. The deeper reason for why this substantial effort is considered wortwhile is to look for a simple yet manageable dynamical formulation of electron transfer processes and the determination of rates of elementary reactions in general. Obviously, time-evolving states are describing chemical transformations and spectroscopic measurements on the molecular and submolecular level. Such states are the solutions of the fundamental time-dependent Schrödinger equation. This equation, rather than the time-independent one, can be transformed between the Schrödinger, Heisenberg, and interaction pictures of quantum mechanics. Currently, the time-independent Schrödinger equation and the determination of its stationary state eigensolutions are receiving the bulk of the attention of the quantum chemists. In particular, the stationary electronic states and their associated potential energy surfaces are theoretical constructs that have occupied quantum chemistry and molecular dynamics since the beginning of quantitative theory. In general, a few adiabatic stationary states and their potential energy surfaces with associated nonadiabatic cou-

 0021-9606/95/103(23)/9968/13/$6.00

pling terms would be necessary to give an accurate description of a dynamical process. Their role is that of a basis for the evolving state. END uses a classical description of the nuclei and attempts to describe the evolving molecular state in a basis of atomic orbitals that move with the nuclei.

One drawback of not using potential energy surfaces and the corresponding stationary electronic states is that one gives up some of the most common and familiar pictures and interpretations used for dynamical events. However, the treatment of dynamics without potential energy surfaces using the direct calculation of evolving states in an arbitrary basis, and their projections onto specific initial or final states, can also be given clear and often striking interpretations. The full dynamical treatment of electrons and nuclei together in a laboratory system of coordinates is, of course, computationally intensive and difficult. One could argue that it is too ambitious an undertaking. However, when compared to the *total* effort of the accurate determination of relevant potential energy surfaces and their couplig terms, appropriate analytical interpolation of the pointwise representation of these surfaces and coupling terms, and the solution of the coupled dynamical equations in a suitable system of internal coordinates, the effort does not look quite as daunting.

The END theory at its simplest level of implementation is presented in the next section followed by a section that describes the results for the $H^+ + H_2$ system and compares them to the experiments and to other theoretical results. A special subsection is devoted to the analysis of product molecule vibrational states. This is important, since the simplest END description employs classical nuclei. The last section offers some concluding remarks and looks towards future applications of the END approach.

II. THE END THEORY

A. Dynamical equations

The electron nuclear dynamics theory[9] employs the time-dependent variational principle to arrive at the dynamical equations for the system. This is a common approach, for instance, the derivation of the equations of classical mechanics from a variational principle is generally considered the most elegant way to arrive at the dynamical equations, either in Hamilton's form or in Newton's form. The power of this approach becomes obvious especially when complex systems are studied. After one has selected the proper degrees of freedom for the problem at hand the variational principle produces the correct set of coupled dynamical equations that determines their evolution in time. There are numerous examples of this approach in all fields of physics and engineering. The first step is the selection of the relevant coordinates q and their velocities $\dot{q}$ or their conjugate momenta p. Next one defines the Lagrangian in terms of coordinates and velocities

$$L(q,\dot{q}) = T(q,\dot{q}) - V(q,\dot{q}), \tag{1}$$

or in terms of coordinates and momenta, incorporating all relevant interactions

$$L(q,p) = \sum_i p_i \dot{q}_i(q,p) - H(q,p)$$

$$= \sum_i p_i \dot{q}_i(q,p) - T(q,p) - V(q,p). \tag{2}$$

The variational principle, making stationary the action with respect to variations in the coordinates and the velocities,

$$\delta A = \delta \int L \, dt = 0, \tag{3}$$

then results in the Euler–Lagrange equations for the system

$$\frac{d}{dt}\frac{\partial L}{\partial \dot{q}} = \frac{\partial L}{\partial q}. \tag{4}$$

These equations become the Hamiltonian equations

$$\dot{q} = \frac{\partial H}{\partial p}, \quad \dot{p} = -\frac{\partial H}{\partial q}, \tag{5}$$

when the variation is performed with respect to the coordinates and the momenta.

Although it has been known since the beginning of quantum mechanics that the Schrödinger equation can be obtained from a variational principle,[11] this approach has not seen much use in the derivation of equations for the dynamics of a complex system. Maybe this is because the dynamical variables, i.e., the coordinates and their conjugate momenta in the fundamental derivation of the Schrödinger equation are the real and imaginary parts of the wave function, which are hard to visualize in order to provide simple physical pictures. There are some examples of this kind of approach for complex systems, for instance, the popular Car–Parinello method[12] is an application of the variational principle, but the need to introduce a fictitious kinetic energy term for the electronic degrees of freedom has resulted in some controversy between proponents and opponents[13] of this approach.

It is, however, perfectly possible to use the variational principle to obtain a consistent set of dynamical equations for all degrees of freedom relevant for the description of a complex system. In chemistry one can obtain a consistent and effective description of a molecular system, by considering the atomic nuclei as classical particles and by treating the electrons quantum mechanically described with a single determinantal wave function

$$|\mathbf{z}\rangle = \det\{\chi_i(x_j)\}. \tag{6}$$

The nuclear positions R and momenta P then form a part of phase space, while the electronic part of phase space is constructed by building the wave function with molecular orbitals

$$\chi_i = u_i + \sum_{j=N+1}^{K} u_j z_{ji} \tag{7}$$

composed of atomic spin orbitals $\{u_i(x)\}$ centered on the nuclei and moving with them. The dynamic variables, i.e., the (generalized) coordinates and momenta, for the electronic degrees of freedom are the complex coefficients $\mathbf{z}=\{z_{ji}\}$. Note that it is essential for the dynamics that the orbital

coefficients are complex, since there must be an imaginary component to play the role of conjugate momentum or velocity. An alternative choice would be the modulus and the phase, but the real and imaginary parts seem to yield the simplest dynamical equations.

Classical nuclei and a single determinantal wave function description of the electrons constitute the simplest model in a possible hierarchy of treatments of molecular systems within the END theory. This model clearly has deficiencies, some of which have been addressed elsewhere[9] with suggestions for generalization, but it has been successful in treating a number of complex processes, including ion-atom and ion-molecule collisions, and intramolecular electron transfer. It actually can be seen as a first step in a systematic procedure that in the end leads to a full quantum mechanical treatment.

The classical treatment of the nuclei can be obtained as the narrow width limit of a nuclear product wave function of Gaussians. A quantum mechanical description of identical nuclei, such as the protons considered here, should, in principle, employ a wave function with proper permutational symmetry. The classical treatment, which neglects such symmetry properties obviously cannot treat, e.g., the forbidden transitions necessary to understand the details of spectroscopy. Another effect is that the narrow wave packet limit puts to zero the exchange terms in the energy, which appear with the proper permutational symmetry. This approximation appears well justified.

Discretization schemes are a natural way of transforming the dynamical equations into a computational problem. The use of grid-point methods, as is done in quantum molecular dynamics, is one such approach. For accuracy, a large number of discretization points is usually needed. In this way, the values of the wave function at discrete points are used as ''coordinates.'' It is difficult to see how to fit a description in terms of such coordinates into a hierarchy of treatments, say, ranging from classical point particles at the simplest level to a full quantum model at the most sophisticated level. The END theory instead utilizes as coordinates (dynamical variables) the average values of the position and the momentum in terms of a chosen wave function form, and a set of complex parameters that describe the shape of the wave function. The theory of coherent states[14–16,5,6,9] provides the mathematical foundation for the choice of such nonredundant dynamical variables, and also for the quantum-classical correspondence, and thus for the construction algorithms yielding a natural hierarchy of coordinates and associated levels of dynamical treatment.

Once the coordinates or the dynamical variables are chosen, the construction of the Lagrangian is straightforward. For END at the simplest level the quantum mechanical electronic Lagrangian is added to the classical Lagrangian for the nuclei to give

$$L=\frac{1}{2}\sum_k (P_k\cdot\dot{R}_k-R_k\cdot\dot{P}_k)-\sum_k \frac{P_k^2}{2M_k} + \langle z|\ \frac{i}{2}\left(\frac{\mathrm{d}}{\mathrm{d}t}-\frac{\tilde{\mathrm{d}}}{\mathrm{d}t}\right)-H_{\mathrm{el}}|z/\langle z|z\rangle, \tag{8}$$

where the tilde on the time differentiation indicates that it acts to the left and where the electronic Hamiltonian H_{el} contains the internuclear Coulombic repulsion terms. Stationarity of the corresponding action leads to the Euler–Lagrange equations in Hamiltonian form[6,9] and to the following set of dynamical equations for the model

$$\begin{pmatrix} i\mathbf{C} & 0 & i\mathbf{C}_R & 0 \\ 0 & -i\mathbf{C}^* & -i\mathbf{C}_R^* & 0 \\ i\mathbf{C}_R^\dagger & -i\mathbf{C}_R^T & i\mathbf{C}_{RR} & -I \\ 0 & 0 & I & 0 \end{pmatrix} \begin{pmatrix} \dot{\mathbf{z}} \\ \dot{\mathbf{z}}^* \\ \dot{\mathbf{R}} \\ \dot{\mathbf{P}} \end{pmatrix} = \begin{pmatrix} \partial E/\partial \mathbf{z}^* \\ \partial E/\partial \mathbf{z} \\ \partial E/\partial \mathbf{R} \\ \partial E/\partial \mathbf{P} \end{pmatrix}. \tag{9}$$

In somewhat more detail these equations can be expressed as

$$\begin{aligned} &\mathbf{C}\dot{\mathbf{z}}+\sum_l \mathbf{C}_{R_l}\dot{\mathbf{R}}_l=-i\,\partial E/\partial \mathbf{z}^*, \\ &\dot{\mathbf{P}}_k+2\ \mathrm{Im}\ \mathrm{Tr}(\mathbf{C}_{R_k}^\dagger\dot{\mathbf{z}})-\sum_l \mathbf{C}_{R_kR_l}\dot{\mathbf{R}}_l=-\nabla_{R_k}E, \\ &\dot{\mathbf{R}}_k=\mathbf{P}_k/M_k. \end{aligned} \tag{10}$$

Here

$$S(\mathbf{z}^*,\mathbf{R},\mathbf{z},\mathbf{R}')=\langle \mathbf{z}|\mathbf{z}\rangle, \tag{11}$$

is the overlap of two determinantal wave functions for different nuclear arrangements, the energy

$$E=\sum_k \frac{P_k^2}{2M_k}+\frac{\langle \mathbf{z}|H_{\mathrm{el}}|\mathbf{z}\rangle}{\langle \mathbf{z}|\mathbf{z}\rangle}, \tag{12}$$

M_k a nuclear mass, and the matrices in the phase space metric are defined as

$$\mathbf{C}=\left.\frac{\partial^2\ \ln S(\mathbf{z}^*,\mathbf{R},\mathbf{z},\mathbf{R}')}{\partial\mathbf{z}^*\partial\mathbf{z}}\right|_{\mathbf{R}'=\mathbf{R}}, \tag{13}$$

$$\mathbf{C}_{\mathbf{R}}=\left.\frac{\partial^2\ \ln S(\mathbf{z}^*,\mathbf{R},\mathbf{z},\mathbf{R}')}{\partial\mathbf{z}^*\partial\mathbf{R}}\right|_{\mathbf{R}'=\mathbf{R}}, \tag{14}$$

and

$$\mathbf{C}_{\mathbf{RR}}=-2\ \mathrm{Im}\left.\frac{\partial^2\ \ln S(\mathbf{z}^*,\mathbf{R},\mathbf{z},\mathbf{R}')}{\partial\mathbf{R}\partial\mathbf{R}'}\right|_{\mathbf{R}'=\mathbf{R}}. \tag{15}$$

In these expressions $\mathbf{z}=\{z_{ji}\}$ denotes a vector array with $(K-N)\times N$ elements.

Detailed expressions of all these quantities have been published.[9] Their evaluation and the integration of the coupled system of dynamical equations are coded in the program system ENDyne.[10]

One can discern the electron-nuclear coupling in the dynamical metric terms. The importance of the coupling terms for the correct description of dynamical events has been studied[8] and their effect on electron transfer probabilities and cross sections documented in some detail.

These equations have now been solved for a number of small collisional systems involving both ionic and neutral atoms and molecules employing modest Gaussian electronic basis sets, and the results have uniformly shown excellent agreement[5–8] with the best experimental studies for transi-

tion probabilities, differential, and total cross sections. It is therefore possible to put a great deal of trust in the results obtained here for the $H^+ + H_2$ collisions.

The applications made so far with the END approach have covered a substantial range of collision energies, from a fraction of an electron volt to several keV, with equal ease. Dynamical approaches that use potential energy surfaces have to include higher stationary energy eigenstates and their potential energy surfaces and coupling terms with increasing collision energy, a complication that has severely restricted applications of many current theoretical approaches. The use of energy eigenstates and potential energy surfaces also introduces the need to employ internal coordinates, which becomes quite forbidding for larger systems and can limit the accuracy of even fully quantum mechanical dynamics.

B. Projection of evolving states

Transition probabilities pertaining to an elementary reaction are obtained by projecting the evolving state corresponding to given initial conditions on various suitable product states. The END evolving state is a Thouless determinant for the participating electrons. Each evolving molecular spin orbital is a linear combination

$$\chi_i = \phi_i + \sum_{j=N+1}^{K} \phi_j z_{ji} \tag{16}$$

of orthonormal molecular spin orbitals $\{\phi_i\}$, which in turn are expressed in nonorthogonal atomic spin orbitals $\{u_i\}$ centered on the dynamically moving nuclei.

Although quite general processes can be studied in this manner within the END approach, it is useful for clarity to specialize here to the case of collisional systems where the product channels consist of at most two fragments. Generalization of the following discussion to situations with more product moieties should be obvious.

The two separating product fragments are labeled A and B, which means that the evolving molecular orbitals can be expressed as

$$\chi_i = \chi_i^A + \chi_i^B \tag{17}$$

and the product fragments are said to be separated when the overlap of the atomic spin orbitals on fragment A with those on fragment B are negligible.

At any given point in time, T, in the evolution after which the separation of products has taken place, a particular molecular product fragment finds itself with some nuclear geometry and its electronic wave function can be projected on an electronic eigenstate of that geometry determined in the same atomic orbital basis. Ideally one should use a full configuration interaction description of such a state, but often a simpler description as that of single excitations only or singles and doubles are found to be sufficient. However, for many processes, as say ion-atom or ion-molecule collisions, one is often only interested in the projections on various charge states, which can be given an even simpler treatment.

The normalized electronic determinantal state vector at time T

$$|\mathbf{z}(T)\rangle / \langle \mathbf{z}(T)|\mathbf{z}(T)\rangle^{1/2} = |\chi_1^A + \chi_1^B \ \chi_2^A + \chi_2^B \ \cdots \ \chi_N^A + \chi_N^B| \langle \mathbf{z}(T)|\mathbf{z}(T)\rangle^{1/2} \tag{18}$$

can be expanded in terms of determinants with different numbers of atomic spin orbitals on each of the two fragments as

$$\begin{aligned} |\chi_1^A + \chi_1^B \ \chi_2^A + \chi_2^B \ \cdots \ \chi_N^A + \chi_N^B| &= \{|\chi_1^A \chi_2^A \cdots \chi_N^A|\} + \{|\chi_1^B \chi_2^A \cdots \chi_N^A| + |\chi_1^A \chi_2^B \cdots \chi_N^A| \\ &\quad + \cdots + |\chi_1^A \chi_2^A \cdots \chi_N^B|\} + \{|\chi_1^B \chi_2^B \cdots \chi_N^A| + \cdots\} \\ &\quad + \cdots + \{|\chi_1^B \chi_2^B \cdots \chi_N^B|\}, \end{aligned} \tag{19}$$

where each curly bracket contains $\binom{N}{M}$ single determinants corresponding to the possible ways of distributing electron charge between the two fragments. Depending on the particular system many of these possibilities may have insignificant weight as obtained from the molecular orbital coefficients. For instance, for neutral or singly charged reactant species only the possibilities of transfer of one or two electrons, and no transfer may have significant weights. At separated products the overlaps between functions of different possible fragmentations vanish.

The transformation between the orthonormal reference molecular spin orbitals $\{\phi_i\}$ and the nonorthogonal atomic spin orbital basis is

$$\phi_i = \sum_j u_j (\mathbf{U}\mathbf{s}^{-1/2})_{ji}, \tag{20}$$

where $\mathbf{U}$ is the unitary transformation that diagonalizes the metric

$$\mathbf{\Delta} = \{\Delta_{ij}\}, \quad \Delta_{ij} = \langle u_i | u_j \rangle, \tag{21}$$

of the atomic orbital basis to form the diagonal matrix

$$\mathbf{s} = \mathbf{U}^\dagger \mathbf{\Delta} \mathbf{U}. \tag{22}$$

This means that the relation

$$u_i = \sum_k \phi_k (\mathbf{s}^{1/2} \mathbf{U}^\dagger)_{ki} \tag{23}$$

holds.

Expanding the (nonorthogonal) evolving molecular orbitals and then also the determinants in Eq. (19) according to these transformations in terms of the orthonormal reference molecular orbitals for, say, fragment C, yields

$$\chi_i^C = \sum_{k,l} \phi_k^C (\mathbf{s}^{1/2} \mathbf{U}^{C\dagger})_{kl} c_{li} = \sum_k \phi_k^C d_{ki}^C \tag{24}$$

and, for example,

$$|\chi_1^A \chi_2^B \cdots \chi_N^B| = \sum_{i_1, i_2, \ldots, i_N} d_{i_1 1}^A d_{i_2 2}^B \cdots d_{i_N N}^B |\phi_{i_1}^A \phi_{i_2}^B \cdots \phi_{i_N}^B|. \tag{25}$$

Since the determinants on the right are orthonormal one can obtain the relevant transition probabilities to particular charge states by simply squaring the coefficients $d_{i_1 1}^A d_{i_2 2}^B \cdots d_{i_N N}^B$, adding them up, and dividing by the total normalization $\langle \mathbf{z}(T)|\mathbf{z}(T)\rangle$.

III. $H^+ + H_2$

A. Experiment and previous theory

From a theoretical point of view, the

$$H_a^+ + H_b H_c(v_i = 0) \tag{26}$$

system of reactants exhibits four distinct processes: The nontransfer (NT) inelastic channel with the products

$$H_a^+ + H_b H_c(v_f), \tag{27}$$

the charge transfer (CT) channel yielding

$$H_a + H_b H_c^+(v_f), \tag{28}$$

the rearrangement (R) or ''reactive'' channels with products

$$H_{b/c}^+ + H_a H_{c/b}(v_f) \tag{29}$$

and

$$H_{b/c} + H_a H_{c/b}^+(v_f), \tag{30}$$

and the collision-induced dissociation (D) channels, producing

$$H_a^+ + H_b + H_c \tag{31}$$

or

$$H_a + H_{b/c}^+ + H_{c/b}. \tag{32}$$

Such a detail is not possible to observe in the experiments used here for comparison. In fact, the established theoretical methods usually make simplifying assumptions that eliminate from consideration some of the channels. For instance, constraints on the range of some interparticle distances will prevent the dynamics to reach the dissociative channels.

The END calculations are compared with results from experimental studies on the NT product channel showing vibrational (rotational) excitation of the H_2 molecule[17–20] and on the charge transfer (CT) channel.[1] Differential cross sections both for scattered protons and hydrogen atoms have been measured at a collision energy of 30 eV in the laboratory frame (20 eV in the center-of-mass frame).

A numer of theoretical models has been applied to this system. The trajectory surface hopping model[2,3] (TSHM) was used for comparison with a time of flight experiment.[1] Disagreements were attributed to unspecified inadequacies of the chosen potential energy surfaces. In particular, the experimental results show a more pronounced angular dependence of the differential cross sections for charge transfer than do the theoretical ones. A quite extensive and elaborate three-dimensional quantum mechanical study of this system[4] employing the DIM surface suggested by Ellison,[21] and invoking the infinite order sudden approximation[4] (IOSA) has been carried out with some better agreement with experiment than that of TSHM. Still, there are discernible differences between some of the results of this study (which will be referred to as IOSA for short) and experiment; particularly, the position of the rainbow angle, and vibrationally resolved differential cross sections deviate from the experimental results. Internal coordinates consisting of the distance R, between the projectile and the center of mass of the target molecule, the bond distance r of the diatomic, and an orientation angle γ, are used in this approach. The discretization of γ, the determination of the limits of R and r, and their influence on the results are said to represent a considerable effort. Yet, it appears that the value chosen for $r_{\max}$ of 2.2 Å excludes any of the processes involving proton exchange, or total breakup, both of which take place at this energy. Furthermore, $R_{\max}=4.7$ Å seems a bit too small a product separation when one of the fragments is charged. Thus, even the three-dimensional quantum mechanical treatment on two coupled surfaces involves a rather constrained dynamics. In view of this, it is interesting to perform the END study of this system with a full dynamics of electrons and nuclei, particularly since the END allows for all possible product channels and does not employ potential energy surfaces.

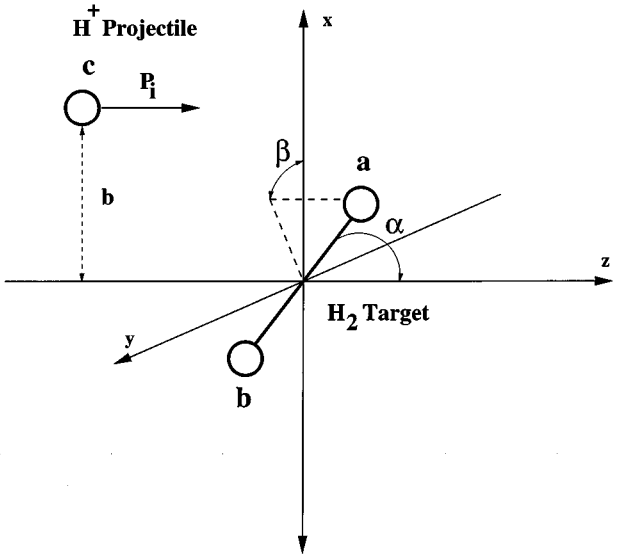

FIG. 1. Reactant initial conditions for the END $H^+ + H_2$ calculations. The nuclei of the H_2 molecule are labeled a and b, respectively (nucleus a with initial x, y, and z positions all $\geqslant 0$), and the H^+ projectile is labeled c. The molecular initial orientation $[\alpha,\beta]$ is given by the polar angle α between the bond and the z axis ($0 \leqslant \alpha \leqslant 180°$), and the azimuthal angle β between the projection of the bond axis in the xy plane and the x axis ($0 \leqslant \beta \leqslant 90°$).

B. Initial conditions and final state analysis

The present END calculations were performed with the ENDyne program package.[10] Parameters defining the initial conditions of the reactants are depicted in Fig. 1. The nuclei originally of the H_2 molecule are labeled a and b, respectively, and the H^+ projectile is labeled c. The electronic state is described in a pVDZ $(4s1p)/[2s1p]$ basis of Dunning[22–24] centered on each of the three nuclei. This basis has shown to be adequate in earlier END studies on hydrogenic systems.[25] The H_2 molecule is initially in its electronic ground state and at its equilibrium geometry as given by the single determinant approximation in the given basis. It is initially at rest with its center of mass at the origin of the laboratory frame. The classical description of the nuclei means that the nuclei are stationary in the vibrational ground state. The H^+ projectile is placed 15 a.u. from the target with a momentum corresponding to E_{lab} 30 eV in the z direction. A number of END trajectories are then calculated for varying

initial orientation $[\alpha,\beta]$ of the target (see Fig. 1) and for different values of the projectile impact parameter b. The values of the polar angle α are chosen in steps of 15° from 0° to 180°, and it was found sufficient to consider only the values 0°, 45°, and 90° for the azimuthal angle β. The impact parameter b assumes values in steps of 0.1 a.u. from 0.0 to 2.0 a.u. and in steps of 0.2 a.u. from 2.0 to 6.0 a.u. Advantage can be taken of the symmetry so that, say, results of an orientation $[\alpha,90°]$ are equivalent to those of the orientation $[180°-\alpha,90°]$. Still the full study involves about 1160 fully dynamical trajectories. Each trajectory evolution ran for 900 a.u. of time in order to achieve full separation of the product fragments. The calculations were performed on an IBM RS/6000-580 computer. The version of the ENDyne code used in this study allowed a total evolution to be carried out in about two hours of CPU time. For example, in the case of the orientation [75°,0°] with an evolution time of 900 a.u., the CPU time decreased steadily from 2.5 h for $b=0.0$ a.u. to 2.0 h for $b=6.0$ a.u.

Each ENDyne run produces the final state of the system of product species, i.e., the final electronic wave function and the final nuclear positions and momenta. From the END evolution selected properties can be calculated with a variety of tools, which are part of the analysis code EVOLVE. For instance, the electronic charge distribution say, as given by the Mulliken population is readily obtained. An analysis of the electronic state is essential in terms of its components that describe the various possible distributions of electronic charge among the separate product species as discussed earlier. Various auxiliary programs make possible further analysis of the large amounts of data generated by the END trajectories. Thus the classical description of the nuclei result in classical differential cross sections with their singularities at rainbow angles and other classical characteristics needing standard semiclassical corrections to compare with experiment. Such semiclassical methods involve the adaptation of the simple nonuniform corrections,[26] also known as the transitional Airy approximation[27] to treat the classical rainbow angles.

Inspection of the END nuclear trajectories, interparticle distances, and atomic charges (Mulliken populations) as function of time permits the determination of the type of process (CT, NT inelastic, etc.). A scattering angle θ is determined as

$$\sin\,\theta=(p_x^2+p_y^2)^{1/2}/p, \tag{33}$$

where $\mathbf{p}=(p_x, p_y, p_z)$ with $p=|\mathbf{p}|$ is the final momentum of the fragment going to the detector (always the fastest).

C. Analysis of vibrational quantum state distributions

Classical nuclei result in the description of a molecular product as a classically vibrating rotor. Nevertheless, a resolution into quantum states can be accomplished[28] by employing coherent states (CS).[14] In order to be specific we consider a diatomic molecule vibrating at some classical frequency ω. Such a classical vibrating object can be described to be evolving in a canonical coherent state[29]

$$|\alpha\rangle=e^{-|\alpha|^2/2}\sum_v\,(\alpha^v/\sqrt{v!})|v\rangle, \tag{34}$$

where α is a continuous complex parameter and $|v\rangle$ are the eigenstates of the harmonic oscillator Hamiltonian of frequency ω. The populations of the various vibrational states are then given by the Poisson distribution

$$P_v=e^{-|\alpha|^2}\,\frac{|\alpha|^{2v}}{v!}. \tag{35}$$

The CS expectation value of the harmonic oscillator Hamiltonian is

$$E_{cs}=\hbar\omega(|\alpha|^2+\tfrac{1}{2}) \tag{36}$$

and the classical nuclei having no zero-point energy vibrate with the energy

$$E=\hbar\omega|\alpha|^2. \tag{37}$$

This part of the product molecule energy is derived from the electron nuclear dynamics, since the total nuclear energy is calculated throughout each trajectory and at final separation can be evaluated for the molecule in question. Subtracting the center of mass translational energy leaves the kinetic energy of the rovibrational motion. In the present case the rotational energy estimated from the angular momentum and the moment of inertia at equilibrium is found to be negligible. The final electronic state of the product molecule comes from projecting, say, the total $H^+ + H_2$ electronic state onto that of H_2. Then the electronic energy of this projected state, possibly an excited state, minus the ground state energy in the given basis yields the excitation energy, which when added to the rovibrational kinetic energy gives the energy E available for quantum vibration and rotation of the molecule.

Therefore the vibrational quantum state distribution of the product molecules becomes

$$P_v=e^{-E/\hbar\omega}\,\frac{(E/\hbar\omega)^v}{v!}. \tag{38}$$

This analysis allows the calculation of a number of vibrationally resolved properties from the END trajectories using classical nuclei. Obviously, the harmonic oscillator CS is adequate only in the case when the first few vibrational levels are significantly populated.

This procedure does not specify the vibrational phase and as such has similarities with a conventional binning procedure used for very large numbers of classical trajectories on a given potential energy surface. However, a binning procedure is not feasible for the small number of fully dynamical END trajectories and the coherent state analysis offers a convenient alternative.

D. END results

The principal assumption in the END theory is that the TDVP yields an appropriate approximation to the time-dependent Schrödinger equation. The approximations then consist of the choice of wavefunction (e.g., Thouless parametrized single determinant and classical nuclei) and that of a basis set. There are no further assumptions about the system

of electrons and atomic nuclei, such as constraints on the range of values for any of the dynamical variables. The electron-nuclear dynamics within these approximations is exact in the sense that the system of coupled differential equations for the dynamical variables is integrated numerically in time to machine precision using standard methods. This approach is capable of describing details of the ''microdynamics'' on electronic time scales, far beyond what is observable with current experimental techniques. Nevertheless, such details give interesting and potentially useful informations about short-time processes. Furthermore, END does not exclude any of the possible processes. In Table I the initial conditions for the $H^+ + H_2$ system are grouped according to which processes are generated. In summary a number of observations can be made.

(i) The dynamics starting from a target orientation $[\alpha,\beta]$ is similar in all respects to that of an orientation $[180°-\alpha,\beta]$. This is expected in view of the rather isotropic interaction between the projectile and the target.

(ii) Effects due to anisotropy of the interaction are mostly apparent for impact parameters below 2.0 a.u. For instance, the rotational excitation, a clear manifestation of such effects, is important in this range.

(iii) The occurrence of dissociation and rearrangements is more prominent for the $[\alpha,0°]$ orientations than for others, and these two channels become less important as α goes to 0° or 180°.

(iv) Initial $[\alpha,0°]$ orientations lead to dissociation and rearrangement for impact parameters less than 1.0–1.5 a.u., while most of $[\alpha,45°]$ and $[\alpha,90°]$ produce the same processes for impact parameters below 0.4–0.8 a.u.

In order to illustrate some detailed END results for the processes listed in Table I, Figs. 2 and 3 depict evolutions for 2000 a.u. of time. The figures refer to the initial target orientation [90°,0°] and impact parameter $b=0.3$, 1.0, and 1.6 a.u. which lead to dissociation, rearrangement, and NT and CT scattering processes, respectively. Figure 2 shows the trajectories of the three nuclei (in the xz plane), and Fig. 3 gives the Mulliken populations vs time. In the dissociation case, the incoming projectile transfers a great deal of momentum inducing the target to dissociate. In this case the outgoing projectile (nucleus a) receives a significant amount of charge from the target molecule. In both the rearrangement and the NT and CT cases, a rovibrationally excited product molecule is being formed. In those cases, the amount of electronic charge transferred is significantly smaller than in the dissociation case. The details in Fig. 4 of the evolution of the three internuclear distances for the NT case indicate that the first change in the target molecule bond distance is the so called bond ''dilution,'' first found in a calculation by Giese *et al.*[30] and also in other treatments[31,1] using classical nuclei.

In the CT scattering case the rovibrational excitation of the target molecule occurs simultaneously with the electron transfer. It is noteworthy in this context that Niedner *et al.* based on their theoretical analysis of the experimental results proposed a two-step mechanism for the CT scattering. An initial step consists of a vibrational excitation of the H_2 molecule to $v_f \geqslant 4$ followed by a second step of electron transfer from the excited molecule. The END dynamics does not support this picture.

TABLE I. Type of process produced by various initial conditions as given by target orientation and projectile impact parameter. *D* denotes dissociation, *R* rearrangement, and NT and CT nontransfer inelastic and charge transfer scattering, respectively.

$[\alpha,\beta]$ target orientation (deg)	END product analysis Impact parameter range (a.u.)	Type of process
[90°,0°]	0.0–0.5	*D*
	0.6–1.1	*R*
	1.2–1.4	*D*
	1.5–6.0	NT and CT
[90°,45°]	0.0–0.5	*D*
	0.6–6.0	NT and CT
[90°,90°]	0.0–0.6	*D*
	0.6–6.0	NT and CT
[60°,0°]	0.0	*R*
	0.1–0.2	*D*
	0.3–1.0	*R*
	1.1–1.3	*D*
	1.4–6.0	NT and CT
[60°,45°]	0.0	*R*
	0.1–0.6	*D*
	0.7–6.0	NT and CT
[60°,90°]	0.0	*R*
	0.1–0.3	*D*
	0.4–6.0	NT and CT
[30°,0°]	0.0–0.1	NT and CT
	0.2–0.9	*D*
	1.0–6.0	NT and CT
[30°,45°]	0.0–6.0	NT and CT
[30°,90°]	0.0–6.0	NT and CT

Another dynamical quantity of interest is the scattering angle, which enters into the expressions for the classical differential cross sections. Ion-molecule collisions are a bit more complex than ion-atom scattering and the determination of a deflection function is not that straightforward. Figure 5 shows the scattering angle as a function of impact parameter for some representative initial reactant orientations. Impact parameter values in Fig. 5 apply only to NT and CT scattering (i.e., no breakup or rearrangement). The maximum in the range of b from 2.0 to 3.0 a.u. can be identified with the primary rainbow angle. Analogous to the case of ion-atom collisions[32,33] this rainbow angle corresponds to the maximum of the attractive part of the interaction between projectile and target. The value of the classical rainbow angle is smallest for the [90°,0°] initial target orientation, and shows a monotonic increase for α going to either to 0° or 180°, or for β approaching 90°. For the [90°,90°] and for all the $[\alpha,0°]$ trajectories a scattering angle of 0°, the glory angle,[32,33] arises for impact parameters smaller than those of the primary rainbow. As is the case for ion-atom collisions, this glory singularity in the classical cross section occurs where the interaction changes from repulsive to attractive. For trajectories with other initial target orientations a nonzero minimum in the scattering angle replaces the glory angle giving rise to a so-called secondary rainbow. This was first described in a DECENT calculation by Giese *et al.*[30] and also found in the TSHM calculations by Niedner *et al.*[1] This

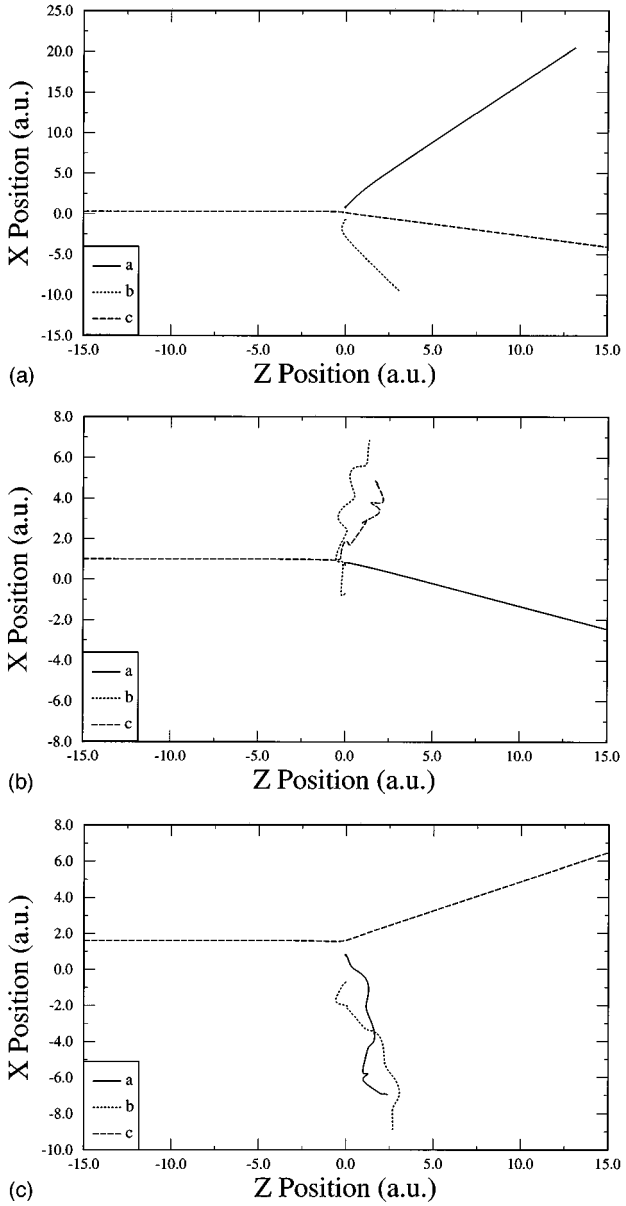

FIG. 2. x vs z position for the three nuclei in three different END $H^+ + H_2$ trajectories, all referring to an initial molecular orientation [90°,0°] for which the dynamics remains in the xz plane. The total evolution time is 2000 a.u. (a) The processes of dissociation (D) at $b=0.3$ a.u.; (b) the rearrangement (R) at $b=1.0$ a.u.; (c) nontransfer/charge transfer (NT/CT) scattering at $b=1.6$ a.u.

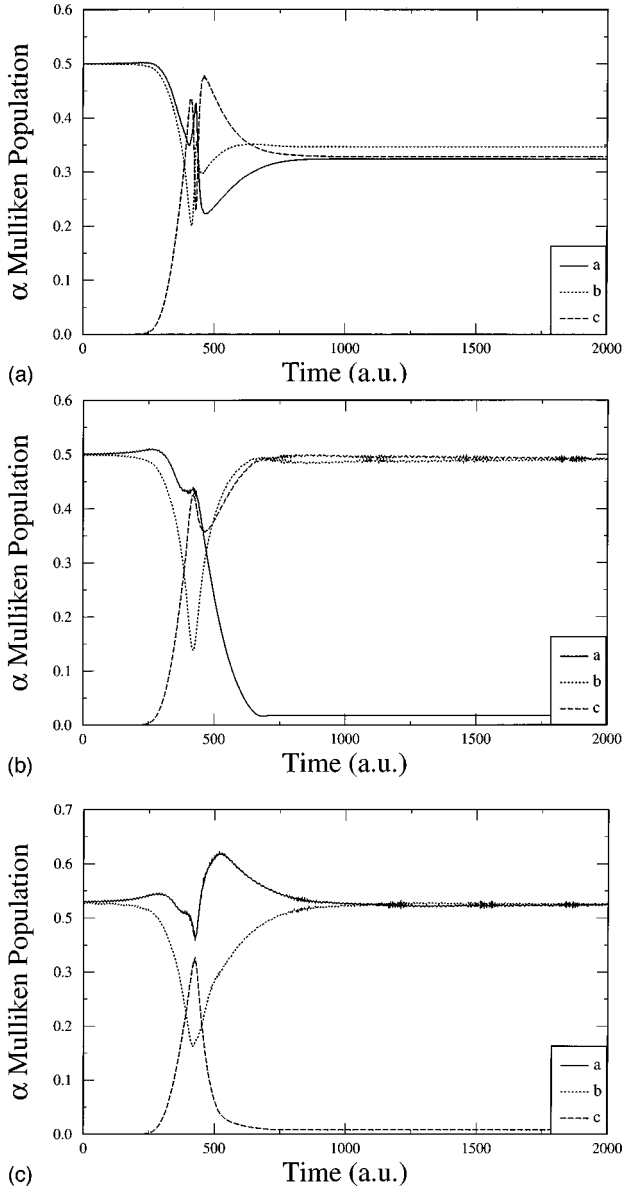

FIG. 3. Mulliken population of α spin electrons vs time for the same three cases as in Fig. 2. The final oscillation of the population in the diatomic fragments reflects their vibrational oscillation after the collision. In the dissociation case (a), the outgoing nucleus c is the fastest and is the one detected in the NT/CT measurement. In (b) and (c) the atomic fragment is faster than the diatomic one and carries the transferred charge.

secondary rainbow is associated with the interaction switching from repulsive to attractive as is the glory angle. For this system it is also associated with the projectile being scattered out of the original xz plane. Actually, its x and y components of momentum pass through zero for close but different values of the impact parameter. Therefore, a zero scattering angle cannot occur, as can be seen from Eq. (33), when the projectile goes from the region of repulsive to the region of attractive interaction. However, the corresponding scattering angle is rather small, which causes a blurring of the rainbow and glory characteristics.

Analysis of the NT and CT probabilities shows that the rearrangement and dissociation processes are most efficient in transferring electronic charge. It is noteworthy that the CT probability as well as the transfer of energy into vibrations both reach a maximum at the impact parameter of the primary rainbow.

Vibrational resolution of various dynamical properties is achieved by subjecting the END trajectories to the analysis using the canonical CS. The result of that procedure for the case of weighted probabilities averaged over all target orientations is shown in Fig. 6. The straight line represents $b\Sigma_i P_i = b$, since the sum over all probabilities must add to unity. The vibrational resolution of the NT channel permits the calculation of the classical vibrationally resolved NT integral cross sections, which show excellent agreement[28] with experiment.

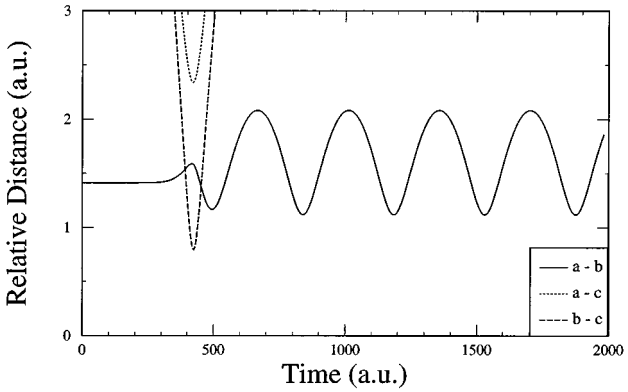

FIG. 4. Relative nuclear distances vs time for the orientation [90°,00°] and impact parameter $b=1.6$ a.u. The bond "dilution" of H_2 as the projectile approaches, the initial vibrational excitation [correlated to the CT process, see Fig. 3(c)], and the vibrational excitation after the collision can readily be discerned.

The NT vibrational energy transfer averaged over all molecular orientations is depicted in Fig. 7 as a function of scattering angle together with the IOSA,[4] the TSHM, and the experimental results.[1] There is a satisfactory agreement with experiment. The structure in the END results is a reflection of the two rainbow angles. Addition of more trajectories would tend to smooth these results.

The calculation of vibrationally resolved differential and integral cross sections is a difficult task for any theoretical method. Obviously, the determination of the classical differential cross sections for non-diatom collisions in general involves two scattering angles [the polar scattering angle θ, as in Eq. (33), and the azimuthal scattering angle ϕ], and the Jacobian J relating the impact parameter b and the azimuthal angle ψ of the projectile with the two scattering angles.[34] The classical differential cross section can be expressed as

$$\mathrm{d}\sigma(\theta,\phi,[\alpha,\beta])/\mathrm{d}\Omega=\sum_i \frac{b_i P_i(\theta,\phi,[\alpha,\beta])}{\sin\ \theta|J_i|}, \tag{39}$$

with

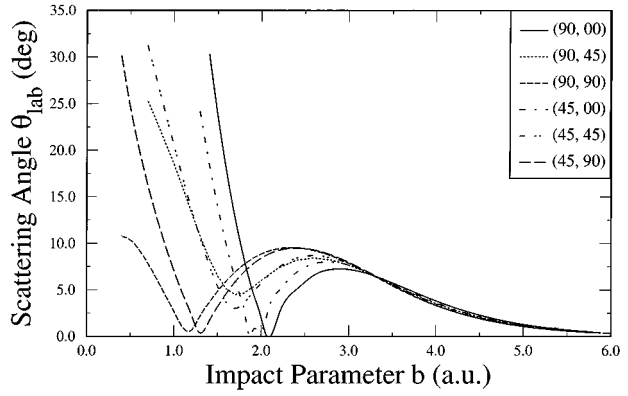

FIG. 5. Laboratory scattering angle θ_{lab} vs impact parameter b for some representative orientations $[\alpha,\beta]$. The cases depicted correspond only to the NT/CT scattering (no dissociation or rearrangement) for sake of simplicity. The primary rainbow angle can be seen for 2.0 a.u.$\leqslant b\leqslant$3.0 a.u. in all cases. In the orientations with $\beta=0°$, a (zero) glory angle can be observed at impact parameters lower than that of the primary rainbow. In the other orientations, a (nonzero) secondary rainbow angle can be seen.

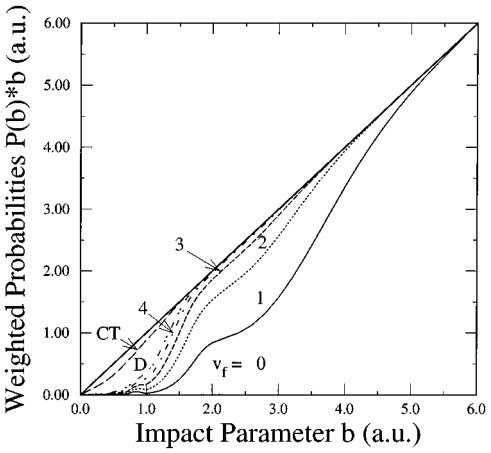

FIG. 6. Orientation-averaged weighted probability vs impact parameter. All the channels shown and $b\Sigma_i P_i(b)=b$ is the upper straight line. CT is total charge transfer via either dissociation or rearrangement or pure scattering, D is nontransfer dissociation, and $v_f=0,1,2,3,4$, final vibrational state of the H_2 molecule in the NT scattering case. The CT probability is a continuous function of the impact parameter but is low at high impact parameter. Observe the predominance of the dissociation and charge transfer processes at low impact parameter, and the higher vibrational excitation at the impact parameters of the primary rainbow.

$$\begin{aligned} J_i&=[\partial(\theta,\phi)/\partial(b,\psi)]_{[\alpha,\beta],b=b_i,\psi=\psi_i},\\ \theta&=\theta(b,\psi),\\ \phi&=\phi(b,\psi), \end{aligned} \tag{40}$$

where the index i runs over all the branches contributing to the scattering direction $[\theta,\phi]$, P_i is the probability of the particular process, and $[\alpha,\beta]$ the initial orientation of the target molecule. However, it is not difficult to prove that for random orientations it suffices to use the Jacobians $j_i=[\partial\theta/\partial b]_{[\alpha,\beta],b=b_i}$ yielding the differential cross section

$$\mathrm{d}\sigma(\theta,[\alpha,\beta])/\mathrm{d}\Omega=\sum_i \frac{b_i P_i(\theta,[\alpha,\beta])}{\sin\ \theta|j_i|}. \tag{41}$$

The classical differential cross sections calculated in this manner provide a good initial estimate of the experimental results in spite of their well-known shortcomings such as the

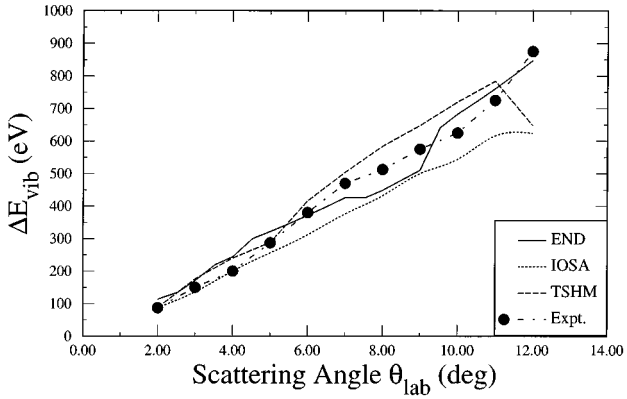

FIG. 7. H_2 NT vibrational energy transfer ΔE_{vib} vs laboratory scattering angle θ_{lab}. Orientation-averaged results from END, IOSA (Ref. 4), and TSHM (Ref. 1) calculations along with experimental data (Ref. 1).

singularities at the rainbow and glory angles, the sudden drop in value in going from the lit to the dark side of a rainbow angle, and the wrong position of the rainbow angle. The average of the END results over the target orientations yields the classical primary rainbow angle at 8.8° as compared to the experimental value somewhere between 6° and 7°. The TSHM result is close to 10°.

Semiclassical corrections are straightforward and yield cross sections that better agree with experiment. An approach first suggested by Ford and Wheeler[26] using the Airy function is employed for the primary rainbow. A key factor is the incorporation of the probabilities for the various processes, a procedure which connects with the exact quantum *T*-matrix formulation of the problems.[32] The END semiclassically corrected primary rainbow angle is 7.2° for the total NT/CT scattering, in excellent agreement with the experimental one. The treatment of the secondary rainbow is less straightforward. There exist in the literature semiclassical treatments of elastic isotropic scattering exhibiting a maximum and a minimum in the deflection function.[35,27,36] The direct application of the uniform Airy approximation to both rainbow angles has been discussed. Approaches based on catastrophe theory, such as the uniform and transitional Pearcey approximations, have been suggested,[36] but it is unclear how pertinent and useful these corrections would be in the present case. No corrections have been made for the secondary rainbow which is the same as done in other studies.[30,1] The averaging procedure of the END smooths the effects of the secondary rainbow, anyway.

Figure 8(a) displays the total NT differential cross section for laboratory scattering angles of 2° through 12°. END is compared to IOSA,[4] TSHM, and the experimental result.[1] The latter has been normalized to the END results by matching the experimental differential cross section at the experimental rainbow to the END total differential cross section at the END rainbow angle. Exactly the same is done in the papers by Niedner *et al.*[1] and Baer *et al.*[4] with their theoretical data. Of course, it makes the other theoretical results appear worse than they really are. Figures 8(b)–8(g), similarly show the vibrationally resolved NT differential cross sections for $v=0,1,2,3,4,5$. The agreement of the END results with experiment is superb with respect to position of the primary rainbow, overall shape, and vibrational resolution. Actually, the position of the END primary rainbow in all cases agrees better with experiment than in the so-called full quantum mechanical study using a DIM surface and the IOSA. The latter predicts cross sections somewhat greater than do either TSHM or END.

The END, IOSA, and TSHM total CT differential cross sections are given in Fig. 9 together with the experimental ones for laboratory scattering angles of 1° through 12°. In fact, the experimental results have been reproduced three times for ease of comparison by normalizing them in turn to the three theoretical curves. The END results again show satisfactory agreement with experiment. The END transfer cross section does better overall than the structureless TSHM results. It also seems to give a better account of the low angle portion than does IOSA, particularly in showing the proper decrease down to 2°.

The END description might be judged less satisfactory at greater scattering angles. The decrease of the theoretical curve is less rapid than the experimental one. The reason for this behavior is understood. For scattering angles greater than the primary rainbow, only the scattered projectiles from the repulsive interaction contribute to the differential cross section. As the scattering angle increases further and the impact parameter decreases, the dissociative region is eventually reached. END shows no dissociation for $\theta \leqslant 12°$. Beyond the primary rainbow angle the CT probability function from the repulsive contributions first decreases but then steeply increases into the region where dissociation dominates. This situation is particularly pronounced for the $[\alpha,90°]$ orientations, which show less repulsion and permits the projectile to get close, interchange a considerable amount of charge, and then scatter. When energy losses higher than 3 eV are excluded the CT differential cross section assumes a fall-off for the higher scattering angles close to experiment. Such a procedure makes sense for the purpose of comparison, since it appears that products suffering these energy losses cannot be seen by experiment.[1]

Vibrational resolution of the CT cross section with the same CS procedure as for the NT channel is not possible within the simplest END model used here. Even though the electronic state is reasonable (as shown by the total differential cross section for charge transfer), the vibrational motion associated with that channel is incorrect. The reason is, of course, that the NT channel dominates and the classical nuclei react to an average force that corresponds mostly to this channel. Hence, the CS vibrational analysis works in that channel, but fails in the charge transfer channel because the END trajectories display a nuclear motion that corresponds more to the H_2 than to the H_2^+ product. The necessary augmentations of the simplest END model in order to remedy this situation will be addressed in a forthcoming paper.

None of the theories, including a multitrajectory method,[37] reproduces the sharp falloff of the experimental differential cross section at very low scattering angles. The END results down to 1° are no different. This increase in the calculated differential cross section for charge transfer seems to have its origin in the secondary rainbow, and particularly involves trajectories with $[\alpha,90°]$ target orientations. Such a pronounced discrepancy between theory and experiment deserves further study.

An intriguing feature of the studies of this simple ion-molecule system is the quite different absolute magnitudes of the total transfer cross section produced by the various theoretical approaches. Unfortunately, the time of flight experiment referred to throughout this study[1] did not yield absolute results, which means that independent investigations must be consulted for comparison. Past experiments on the CT processes of $H^+ + H_2$ measured only integral cross sections, and most of those experiments were not carried out at energies close to $E_{lab}=30$. Some experiments at 30 eV actually failed to detect any transfer whatsoever.[38] Therefore, the value used here for comparison is one interpolated from data compiled by Phelps.[39] This data collection contains quite a few experimental results for $23.16\ \text{eV} \leqslant E_{lab} \leqslant 10\,000\ \text{eV}$. Among these data, the experiment closest to our collision energy is the one

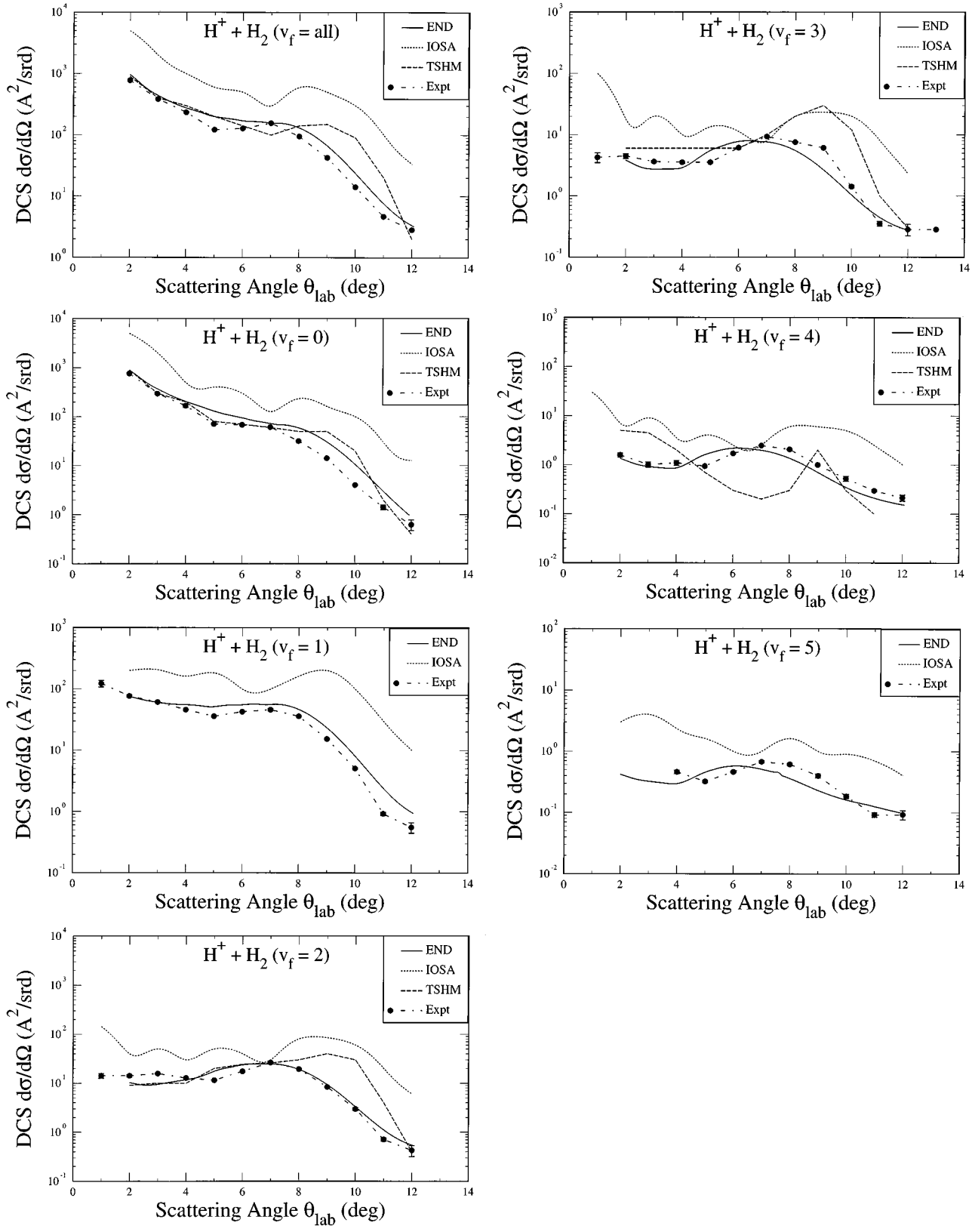

FIG. 8. Nontransfer differential cross sections vs laboratory scattering angle for different final vibrational states. Orientation-averaged results from END, IOSA (Ref. 4), and TSHM (Ref. 1) along with experiment (Ref. 1). The latter have been normalized to the END results by matching the experimental total NT differential cross section at the experimental rainbow angle. The total and the vibrationally resolved differential cross sections for $v_f = 0$, 1, 2, 3, 4, and 5 are shown.

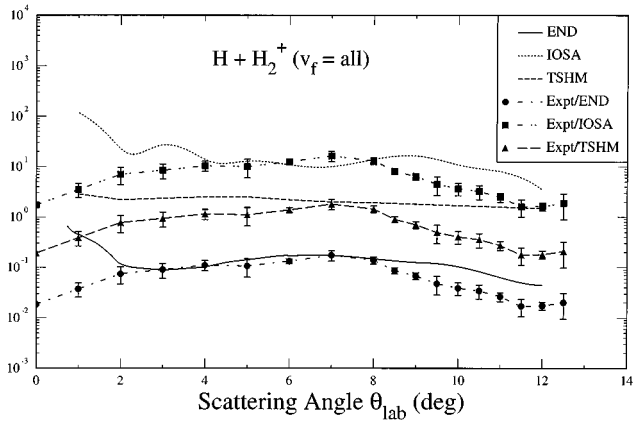

FIG. 9. Charge transfer total differential cross sections vs. laboratory scattering angle. Orientation-averaged results from END, IOSA (Ref. 4), and TSHM (Ref. 1) calculations along with experimental results (Ref. 1) normalized to the three calculations.

by Gealy *et al.*[40] The fitted values are also consistent with those in the classical works by Cramer[38] and Koopman.[41] Table II compares the interpolated experimental CT cross sections with the available theoretical ones. The END values are obtained by

$$\sigma([\alpha,\beta])=\int_{b_1}^{b_2}P(b,[\alpha,\beta])b\,db \tag{42}$$

followed by an average over orientations. The integration limits are chosen to correspond to the scattering angle interval of interest. It is not possible to ascertain whether the experimental values include dissociation and rearrangement contributions to the total CT process. Therefore, Table II contains three different columns: (i) $0\leqslant\theta_{\rm lab}\leqslant 12°$ the span of scattering angle in the experiment of Niedner *et al.*[1] END does not predict dissociation or rearrangement in this range. (ii) The full range of scattering angle but excluding the contributions from dissociation and rearrangement, i.e., scattering CT integral cross section. (iii) The full range of scattering angle with all contributing processes included (dissociation, rearrangement, and scattering), i.e., the full CT integral cross section.

IV. CONCLUSIONS

With every new application of the END theory more is revealed about the power and limitations of its formulation in the simplest terms, i.e., a single determinantal state for the electrons and classical nuclei. Obviously, one would expect there to be situations which would demand a quantum mechanical description of the nuclei. Nevertheless, this simplest END model has shown surprising resilience and ability to give excellent results for small collisional systems that exhibit a great variety of competing processes. The END results for the $H^+ + H_2$ reaction presented here using a modest pVDZ basis are, in most respects, superior to those of competing theoretical approaches. The results presented here and elsewhere using the ENDyne code provide evidence that the correct treatment of electron-nuclear coupling is important for these dynamical processes and also shows that there exist convenient direct paths to dynamics that avoid the detour through stationary electronic states and potential energy surfaces.

However, it is also clear that further development of the simplest END model is necessary in order to treat all the details of a system as $H^+ + H_2$ at 30 eV. As discussed earlier, the classical description of the nuclei is not flexible enough to permit a reasonable vibrational resolution of the charge transfer cross sections. The dominant NT dynamics establishes the character of the nuclear trajectories and in order to yield the correct detailed dynamics for the charge transfer, which has a small probability, one could introduce a split wave packet description. Such a formulation can also be taken to the narrow wave packet (or classical) limit. Work in this direction is already started an will be reported in a forthcoming paper.

TABLE II. The integral charge transfer cross section in Å^2 calculated in three different ways and compared to experiment. IOSA refers to Baer *et al.* (Ref. 4), TSHM to Niedner *et al.* (Ref. 1), and the experiment an interpolated value from Phelps (Ref. 39).

Method	$0°\leqslant\theta_{\rm lab}\leqslant 12°$	All $\theta_{\rm lab}$ excluding D and R	All $\theta_{\rm lab}$ all processes
IOSA	0.73		1.10
TSHM			0.3
END	1.44×10^{-2}	0.121	0.275
Experiment			0.371

ACKNOWLEDGMENTS

We thank Pete Haaland for bringing this problem to our attention. Support from the Office of Naval Research is gratefully acknowledged.

[1] G. Niedner, M. Noll, J. Toennies, and Schlier, J. Chem. Phys. **87**, 2686 (1987).
[2] A. Bjerre and E. E. Nikitin, Chem. Phys. Lett. **1**, 179 (1967).
[3] J. C. Tully and R. K. Preston, J. Chem. Phys. **55**, 562 (1971).
[4] M. Baer, G. Niedner-Schatteburg, and J. P. Toennies, J. Chem. Phys. **91**, 4169 (1989).
[5] Y. Öhrn *et al.*, in *Time Evolution of Electrons and Nuclei in Molecular Systems*, in *Time-Dependent Quantum Molecular Dynamics*, edited by J. Broeckhove and L. Lathouwers (Plenum, New York, 1992), pp. 279–292.
[6] E. Deumens, A. Diz, H. Taylor, and Y. Öhrn, J. Chem. Phys. **96**, 6820 (1992).
[7] R. Longo, E. Deumens, and Y. Öhrn, J. Chem. Phys. **99**, 4554 (1993).
[8] R. Longo, A. Diz, E. Deumens, and Y. Öhrn, Chem. Phys. Lett. **220**, 305 (1994).
[9] E. Deumens, A. Diz, R. Longo, and Y. Öhrn, Rev. Mod. Phys. **66**, 917 (1994).
[10] E. Deumens, A. Diz, and H. Taylor, *Manual for the Electron Nuclear Dynamics Software ENDyne* (QTP, University of Florida, Gainesville, FL., 1992).
[11] P. A. M. Dirac, Proc. Cambridge Philos. Soc. **26**, 376 (1930).
[12] R. Car and M. Parrinello, Phys. Rev. Lett. **55**, 2471 (1985).
[13] D. K. Remler and P. A. Madden, Mol. Phys. **70**, 921 (1990).
[14] J. R. Klauder and B.-S. Skagerstam, *Coherent States, Applications in Physics and Mathematical Physics* (World Scientific, Singapore, 1985).
[15] D. J. Thouless, Nucl. Phys. **21**, 225 (1960).
[16] E. Deumens and Y. Öhrn, J. Mol. Struct. (Theochem) **199**, 23 (1989).
[17] H. Udseth, C. F. Giese, and W. Gentry, Phys. Rev. A **8**, 2483 (1973).
[18] J. R. Krenos, R. K. Preston, R. Wolfgang, and J. C. Tully, J. Chem. Phys. **60**, 1634 (1974).
[19] K. Rudolph and J. P. Toennies, J. Chem. Phys. **65**, 4483 (1976).
[20] V. Hermann, H. Schmidt, and F. Linder, J. Phys. B **11**, 493 (1978).

[21] F. O. Ellison, J. Am. Chem. Soc. **85**, 3540 (1963).
[22] T. H. Dunning, Jr., J. Chem. Phys. **90**, 1007 (1989).
[23] T. H. Dunning, Jr., J. Chem. Phys. **53**, 2823 (1970).
[24] S. Huzinaga, J. Chem. Phys. **42**, 1293 (1965).
[25] R. Longo, Ph.D. thesis, University of Florida, Gainesville, FL, 1993.
[26] K. W. Ford and J. A. Wheeler, Ann. Phys. **7**, 259 (1959).
[27] J. N. L. Connor, in *Semiclassical Methods in Molecular Scattering and Spectroscopy*, Vol. 53 of Nato Advanced Study Institute Series, edited by M. S. Child (Reidel, Dordrecht, 1979).
[28] J. A. Morales, A. C. Diz, E. Deumens, and Y. Öhrn, Chem. Phys. Lett. **233**, 392 (1995).
[29] C. Cohen-Tannoudji, B. Diu, and F. Laloë, *Quantum Mechanics* (Wiley-Interscience, New York, 1977), Vol. 1.
[30] C. Giese and W. R. Gentry, Phys. Rev. A **10**, 156 (1974).
[31] H. Krüger and R. Schinke, J. Chem. Phys. **66**, 5087 (1977).
[32] M. S. Child, *Molecular Collision Theory* (Academic, London, 1974).
[33] R. G. Newton, *Scattering Theory of Waves and Particles* (Springer-Verlag, New York, 1982).
[34] E. A. Gislason, Chem. Phys. Lett. **42**, 315 (1976).
[35] J. N. L. Connor, Mol. Phys. **26**, 1217 (1973).
[36] J. N. L. Connor and D. Farrelly, J. Chem. Phys. **75**, 2831 (1981).
[37] A. Florescu, M. Sizun, and V. Sidis, J. Chem. Phys. **99**, 7277 (1993).
[38] W. H. Cramer, J. Chem. Phys. **35**, 836 (1961).
[39] A. V. Phelps, J. Phys. Chem. Ref. Data **19**, 653 (1990).
[40] M. W. Gealy and B. V. Zyl, Phys. Rev. A **36**, 3091 (1987).
[41] D. Koopman, Phys. Rev. **154**, 154 (1966).